Journal of Genetic Engineering and Biotechnology 23 (2025) 100531

Contents lists available at ScienceDirect

Journal of Genetic Engineering and Biotechnology

journal homepage: www.elsevier.com/locate/jgeb

Computational identification of dual COX-1 and NIK inhibitors from marine microalga *Chlorella vulgaris*

Mahesh Samantaray [a,b,1], Sthitaprajna Sahoo [c,1], Durga Prasad Sahoo [d], Guneswar Sethi [e], Sarman Singh [a], Hak-Kyo Lee [c,f], Biswajita Pradhan [g,h,*], Donghyun Shin [c,*]

[a] Directorate of Medical Research, Aarupadai Veedu Medical College & Hospital, Puducherry 607403, India
[b] Department of Bioinformatics, Pondicherry University, Puducherry 605014, India
[c] Department of Agricultural Convergence Technology, Jeonbuk National University, Jeonju 54896, Republic of Korea
[d] Department of Radiation Oncology, Acharya Harihar PG Institute of Cancer, Cuttack 753007 Odisha, India
[e] Center for Large Animals Convergence Research, Korea Institute of Toxicology, Jeongeup-si, Jeonbuk-do 56212, Republic of Korea
[f] Department of Animal Biotechnology, Jeonbuk National University, Jeonju, Republic of Korea
[g] School of Biological Sciences, AIPH University, Bhubaneswar, Odisha, India
[h] Department of Botany, Model Degree College, Rayagada 765017 Odisha, India

ARTICLE INFO

Keywords:
Anti-inflammation
In silico
Molecular docking
Molecular dynamic simulation
GC-MS

ABSTRACT

The search for safe and effective anti-inflammatory agents remains a critical area of research due to the widespread impact of chronic inflammatory diseases. Natural compounds, particularly those derived from marine sources, present a promising avenue for developing novel therapeutics. In this study, we investigated the potential of *Chlorella vulgaris*, a unicellular green alga with a rich profile of bioactive compounds, as a source of anti-inflammatory agents. Through *in silico* molecular docking and dynamics simulations, we identified compounds C8 and C4 as potent inhibitors of COX-1 and NIK, key targets in inflammatory pathways. These compounds demonstrated significantly stronger binding affinities than standard inhibitors MXM and OWC. For COX-1, C8 and C4 showed binding affinities of −8.625 and −4.359 kcal/mol, respectively, compared to −3.454 kcal/mol for MXM. Similarly, for NIK, the binding affinities were −6.798 and −3.789 kcal/mol for C8 and C4, respectively, compared to −2.628 kcal/mol for OWC. Molecular dynamics simulations further demonstrated that C8 and C4 formed stable interactions, including hydrogen bonds and hydrophobic contacts, with key residues in the active sites of COX-1 and NIK, suggesting a potential for sustained inhibitory activity. These findings highlight the therapeutic potential of *C. vulgaris* derived compounds for the treatment of inflammatory conditions. Although further in vitro and in vivo studies are necessary to fully elucidate their efficacy and safety, these results provide a promising foundation for the development of novel, naturally sourced anti-inflammatory therapies.

1. Introduction

Inflammatory diseases arise from dysregulation of the immune system, leading to its inappropriate targeting of self-tissues. It is typically classified into two categories acute and chronic inflammation. While acute inflammation represents a physiological response to injury or infection, characterized by pain, heat and erythema but chronic inflammation develops when this response persists, potentially damaging healthy tissues. This sustained inflammatory state is implicated in a range of pathologies, including rheumatoid arthritis, Crohn's

Abbreviations: COX-1, Cyclooxygenase-1; NIK, NF-κB-Inducing Kinase; ADMET, Absorption, Distribution, Metabolism, Excretion, and Toxicity; H-bond, Hydrogen Bond; kcal/mol, Kilocalories per Mol (unit of binding energy); Lipinski's Rule, Lipinski's Rule of Five (drug-likeness criteria); RMSD, Root mean square deviation; RMSF, Root mean square fluctuations; Rg, Radius of gyration; SASA, Solvent accessible surface area; PCA, Principal component analysis; FEL, Free energy landscape; MM-PBSA, Molecular Mechanics – Poisson-Boltzmann Surface Area.

* Corresponding authors at: School of Biological Sciences, AIPH University, Bhubaneswar, Odisha, India (B. Pradhan); Department of Agricultural Convergence Technology, Jeonbuk National University, Jeonju 54896, Republic of Korea (D. Shin).
E-mail addresses: pradhan.biswajita2014@gmail.com (B. Pradhan), sdh1214@gmail.com (D. Shin).
[1] Both authors contributed equally and shared the first authorship.

https://doi.org/10.1016/j.jgeb.2025.100531
Received 8 April 2025; Received in revised form 14 June 2025; Accepted 24 June 2025
Available online 30 June 2025
1687-157X/© 2025 The Authors. Published by Elsevier Inc. on behalf of Academy of Scientific Research and Technology. This is an open access article under the CC BY-NC-ND license (http://creativecommons.org/licenses/by-nc-nd/4.0/).

disease, lupus, cardiovascular disease, diabetes, cancer, and Alzheimer's disease.[1–3] Enzymes such as COX-1, COX-2, 5-LOX, 15-LOX, and NF-κB play crucial roles in inflammatory processes.[4–8]

Cyclooxygenase-1 (COX-1) plays a critical role in the inflammatory process by transforming arachidonic acid into lipid mediators implicated in inflammation, such as prostaglandins and thromboxane.[9] Several tissues constitutively express COX-1, which is in charge of preserving regular physiological processes like kidney blood flow regulation and stomach lining protection.[10] Nevertheless, COX-1 helps produce pro-inflammatory prostaglandins during inflammation, intensifying inflammatory reactions. Knowing how COX-1 contributes to inflammation aids in the creation of focused treatments for inflammatory diseases. COX-1 is distinct from COX-2, another isoform of the enzyme mainly produced in inflammatory areas and inducible. Traditional nonsteroidal anti-inflammatory medicine (NSAIDs) inhibit both COX-1 and COX-2, resulting in a wider spectrum of effects, whereas COX-2 inhibitors are intended to reduce inflammation without impacting COX-1.[11,12] An NSAID called meloxicam (MXM) is used to treat rheumatoid arthritis and osteoarthritis by reducing pain and inflammation. It functions by preventing the cyclooxygenase (COX) enzyme from producing prostaglandins, which are responsible for pain and inflammation.[13,14] However, like other NSAIDs, Meloxicam can have common side effects, i.e., diarrhea, nausea, stomach pain, dizziness, and indigestion.[15] Apart from this, it also causes more serious side effects such as stroke or heart attack, especially in individuals with pre-existing heart conditions or long-term use. It can also cause gastrointestinal bleeding, which can be fatal. Additionally, it also causes some other serious side effects, which include liver and kidney damage.[13,14]

NF-κB-inducing kinase (NIK) regulates the noncanonical NF-κB pathway, a critical regulator of inflammation and immune responses. NIK mediates diverse cellular processes, including differentiation, proliferation, and survival. Aberrant NIK expression or regulation has been implicated in cancer, metabolic disorders, and various inflammatory diseases.[16] In inflammatory disorders, NIK modulates endothelial cell activation, leading to increased immune cell adhesion and the subsequent exacerbation of inflammation through the upregulation of inflammatory mediators and adhesion molecules.[17] Consequently, NIK inhibition offers a potential therapeutic avenue for the treatment of chronic inflammatory diseases by targeting these key pathways. Compound OWC, chemically known as (2R)-4-[1-(2-amino-5-chloropyrimidin-4-yl)-2,3-dihydro-1H-indol-6-yl]-2-(1,3-thiazol-2-yl) but-3-yn-2-ol, acts as an inhibitor of the NF-κB pathway. By inhibiting this pathway, compound OWC may attenuate inflammation and modulate immune responses, suggesting its potential therapeutic utility in inflammatory diseases. Mechanistically, OWC inhibits NF-κB activation by preventing its nuclear translocation, thereby suppressing the expression of pro-inflammatory genes.[18] While this inhibitory action may offer therapeutic benefits in mitigating chronic inflammation, a key feature of inflammatory conditions such as rheumatoid arthritis and inflammatory bowel disease, potential adverse effects associated with OWC warrant careful consideration. Similar to other NF-κB inhibitors, OWC may induce gastrointestinal disturbances, including nausea, vomiting, and diarrhea. Moreover, prolonged use, analogous to Meloxicam, may elevate the risk of cardiovascular complications such as stroke and myocardial infarction. The immunosuppressive potential of NF-κB inhibition also raises concerns regarding increased susceptibility to infection.

Many synthetic anti-inflammatory drugs, like NSAIDs, can cause side effects such as gastrointestinal issues, cardiovascular problems, and kidney damage.[19] Natural anti-inflammatory compounds are often part of a broader approach to health that includes diet, lifestyle, and overall wellness. Foods like fatty salmon, berries, and green leafy vegetables contain compounds that help reduce inflammation. Particularly in areas where access to synthetic medications is restricted, natural compounds may be more accessible and more sustainable. Since they may be sourced from regional foods and plants, they are a sensible choice for many people.[20] In this regard, the search for natural compounds is promising as they have fewer side effects. Marine algae, particularly, have garnered significant attention due to their potential as sources of bioactive compounds with various health benefits.[21–26] *Chlorella vulgaris* is a unicellular green microalga known for its rich composition of bioactive metabolites, including polysaccharides, carotenoids, and polyunsaturated fatty acids,[27] which displayed several biological activities such as antimicrobial, antioxidant, and anti-inflammatory effects.[27] Among these, anti-inflammatory compounds are of particular interest due to their potential applications in treating inflammation-related conditions.

Keeping this in view, this study aims to identify and profile the anti-inflammatory compounds present in *C. vulgaris* using Gas Chromatography-Mass Spectrometry (GC-MS). GC-MS-based chemical profiling enables detailed characterization of these compounds, elucidating their chemical structures and potential therapeutic properties.[28,29] In silico approaches, such as molecular docking and virtual screening,[29] were performed to predict interactions between the compounds derived from *C. vulgaris* and specific inflammatory targets, such as COX-1 and NIK. This enhances our understanding of the molecular mechanisms underlying their anti-inflammatory effects and aids in identifying novel compounds with high therapeutic potential. The integration of computational techniques with traditional biochemical methods offers a promising approach for developing novel anti-inflammatory agents from marine microalgae. This research has the potential to advance therapeutic strategies and enhance our understanding of inflammatory disease management. *C. vulgaris* represents a valuable resource for natural anti-inflammatory compounds, potentially leading to the development of novel therapeutics.

2. Methodology

2.1. Collection of datasets

Crystal structures of COX1 and NF- κB were retrieved from the RCSB Protein Data Bank database (https://www.rcsb.org/). The crystal structure of COX1 (PDB ID: 4O1Z) comprises 553 amino acid residues and contains a co-crystalized ligand, Meloxicam (MXM), a partial inhibitor of COX1.[30] Similarly, the NF- κB inducing kinase (NIK) crystal structure comprises 342 amino acids with a co-crystalized ligand, OWC.[31] The missing residues in the crystal structure of NIK (residues S38-E51 and Q218-I232) were predicted using the Swiss-Model web server.[32] The water and other small molecules were removed from both proteins.

A GC-MS analysis of the methanolic extract from *C. vulgaris* was performed, presented in our previous publication,[28] and also provided in Supplementary Table S1. The GC-MS results exhibited 14 different peaks of potential compounds at different retention times. Hence, these 14 compounds were retrieved in.sdf format from the PubChem database and considered further for molecular docking analysis. The drug-like properties of these compounds were mentioned in our previous study.[28]

2.2. Molecular docking

To identify the most potent natural compound from *C. vulgaris* against both the targets, i.e., COX-1 and NIK, we performed molecular docking studies using the Schrodinger Maestro 2024–3 package. The proteins were prepared using the protein preparation wizard, permitting the standard protocols. Protonation states were adjusted using PROPKA at physiological pH (7.4). The dimension of the grid box for both receptors was generated (using Receptor Grid Generation) according to the position of the crystalline ligands. The grid box dimensions were set to 30 × 30 × 30 Å for both the receptors. The grids center at 239.81, 113.85, 42.81 for COX-1 and 28.02, 55.38, 5.77 for NIK. All the algal-derived compounds and crystallized ligands were prepared using the LigPrep module. Ten optimal conformations for each ligand were

generated and docked with both receptors using the XP (extra-precision) approach. The XP (extra precision) method in Schrodinger's Glide module offers higher discriminatory power and penalizes non-physical ligand-receptor interactions more rigorously than SP (standard precision). The glide gscore function was used to evaluate the binding affinity and interaction between the receptors and ligands. The ADMET properties of the lead compounds C4 and C8 were evaluated using the SwissADME web server[33] and systematically compared with the reference drugs Meloxicam (MXM) and OWC to assess their drug-likeness, pharmacokinetic profiles, and oral bioavailability.

2.3. Molecular dynamics protocols

Two selected algal-derived compounds and the respective crystalized ligands of both the receptors (3 protein–ligand complexes with each receptor; a total of 6 complexes) were considered for all-atom molecular dynamics (MD) simulations. MD simulations were performed using the Gromacs 2022.2 package and CHARMM36 force field parameters.[34–36] The optimized ligand structures and their corresponding topology files were generated using the CGenFF webserver.[37] The systems were further solvated using the TIP3P water model and a cubic box type with a minimum distance of 1.0 nm between the solute and box edge. Sodium and chlorine ions were added to neutralize the system. The Steepest-descent algorithm was used to perform energy minimization of the system with a maximum tolerance of 1000 kJ/mol/nm.[38] Next, all the systems were equilibrated using a Berendsen thermostat (V-rescale) and Parrinello-Rahman pressure coupling algorithm at 300 K and 1 Pascal bar pressure, respectively.[39,40] All the systems were equilibrated for 100 ps each under NVT and NPT conditions. Finally, a 100 ns MD simulation was performed for all systems, and trajectories were saved at a 2 fs interval. The whole trajectory information was used to study the root mean square deviation (RMSD) of backbone atoms of the receptors and ligands, root mean square fluctuation (RMSF), radius of gyration (Rg), and solvent accessible surface area (SASA) using GOMACS's modules. Secondary structure assignments were computed using the gmx do_dssp module integrated within the GROMACS package. The initial 50 ns trajectory was considered as equilibrated states, and the last 50 ns trajectory information was used to study the global dynamics of both receptors induced by each ligand, as reported in our previous studies.[41–43]

2.4. PCA based FEL analyses

We utilized Principal Component Analysis (PCA) to analyze molecular dynamics trajectories, uncovering major conformational changes. The GROMACS *g_covar* module generated a covariance matrix, which *g_anaeig* then diagonalized to yield eigenvalues and eigenvectors (principal components). We assessed the top five PCs for cosine content; values under 0.2 indicated excellent sampling convergence and biological significance. This led us to select PC1 and PC2 for constructing Gibbs free energy landscapes (FEL) using the *g_sham* utility. These 2D FELs were visualized and analyzed with Mathematica, as mentioned in our previous study.[44] From these landscapes, we identified global energy minima, representing the most stable conformations across six different complexes. This approach allowed us to effectively compare their structural dynamics and infer potential functional roles.

2.5. Binding free energy calculation

MM-PBSA is a widely used computational approach for calculating the binding free energy of biomolecular complexes, including protein–ligand complex, protein-DNA, protein-RNA, and protein–protein interactions.[45] It is extensively employed in computer-aided drug discovery and lead optimization to assess ligand binding affinities, compare binding poses, and guide the selection of potential drug candidates. This approach integrates molecular mechanics, solvent model, and empirical solvation energy terms to provide insights into protein–ligand interactions. The current study calculated the systems' binding free energy (ΔG) using the *g_mmpbsa* module by considering 50 ps coordinates from the last 50 ns MD simulation trajectories.[46]

3. Results and discussion

3.1. Binding interactions of algal-derived compounds with COX1 and NIK

The Schrodinger Maestro 2024–3 was employed for the XP (Extra Precision) docking studies and the prediction of molecular docking energy values, including the docking and Glide scores. Glide energy focuses on the energy associated with the interactions between the ligand and receptor, accounting for intermolecular forces such as hydrogen bonding, hydrophobic interactions, electrostatic interactions, and van der Waals forces.

All the screened compounds were docked against COX-1 and NIK and sorted based on their docking scores in Table 1. The data provides a detailed comparison of the receptor-ligand interactions between the potential natural compound from *C. vulgaris* and the approved drugs against COX-1 and NIK. The bond distances between the key amino acid residues and the compounds were analyzed to assess selectivity and binding strength, focusing on identifying compounds that exhibit stronger interactions with COX-1 and NIK (Fig. 1). Hydrogen bonding, hydrophobic interactions, and salt bridges, highlighted by certain amino acid interactions, play a crucial role in stabilizing these protein-inhibitor complexes.

Compounds such as C6, C8, C5, C9, C2, C4, C7 and C11 exhibited a binding affinity of −9.311, −8.625, −7.925, −7.035, −5.971, −4.349, −4.102 and −3.993 kcal/mol, respectively compared to the standard compound which is MXM having a binding energy of −3.454 kcal/mol with the COX-1. Additionally, compounds C8, C10, C7, C4, C1, C6, and C9 exhibited a binding energy of −6.798, −5.291, −4.955, −3.789, −3.699, −3.248 and −3.230 kcal/mol, respectively compared to the standard compound, OWC having a binding energy of −3.454 kcal/mol with the NIK receptor. Among the 9 listed compounds, C8 and C4 emerged as the standout candidates, highlighting their potential as highly selective inhibitors in molecular docking analysis. These compounds demonstrate potential for selective inhibition, and their absolute binding energy values compared with the standard compound suggest that they require further analysis for effectiveness. MXM, the reference compound for COX-1, demonstrated H-bond interaction with S530 by forming a bond as short as 3.2 Å. As compared to C4, C8 has a higher binding affinity with COX-1. While C8 formed one H-bond with R120 and one salt-bridge interaction with Y355, C4 formed two H-bonds with Y385 and S530. Y355, at the cyclooxygenase channel entrance, is known to interact with NSAIDs like ibuprofen. This C8-Tyr355 interaction highlights a shared pharmacophoric element with established NSAIDs, indicating a similar binding strategy. Additionally, C8 and C4 established 12 and 7 hydrophobic interactions with the COX-1 receptor, respectively. Although C8 has a stronger binding score with the COX-1,

Table 1
The binding affinity of all the algal-derived compounds and co-crystallized ligands (MXM and OWC) against anti-inflammatory receptors, COX-1 and NIK.

COX-1		NIK	
Compounds	Glide score	Compounds	Glide score
C6	−9.311	C8	−6.798
C8	−8.625	C10	−5.291
C5	−7.925	C7	−4.955
C9	−7.035	C4	−3.7894
C2	−5.971	C1	−3.699
C4	−4.359	C6	−2.248
C7	−4.102	C9	−3.230
C11	−3.993	OWC	−2.628
MXM	−3.454	C2	−2.614
C1	−2.660	C13	−2.552

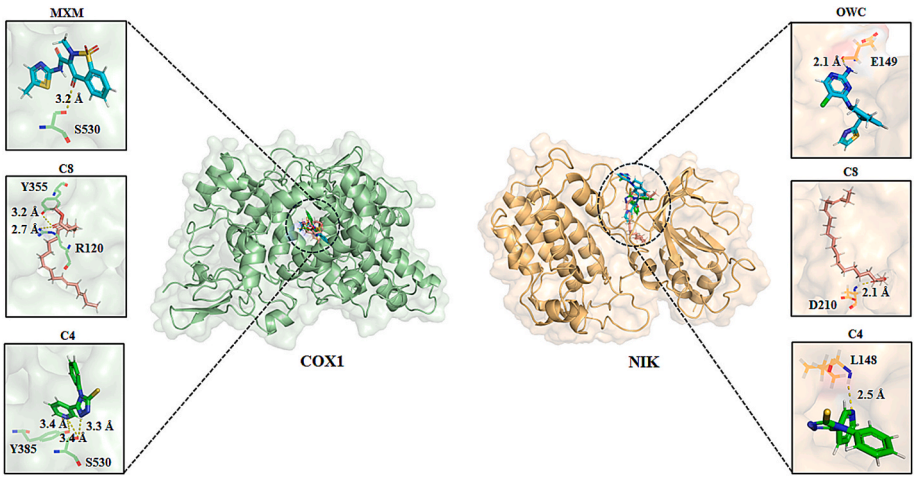


Fig. 1. Molecular interaction of selected compounds with COX-1 and NIK. The pale green and light orange color cartoon structures represent the COX-1 and NIK receptors, respectively. Both the reference compounds (MXM and OWC) are represented with a cyan stick model and interacting residues were highlighted with lines. (For interpretation of the references to color in this figure legend, the reader is referred to the web version of this article.)

C4 formed two strong H-bond interactions and one with the S530 residue, which also formed an H-bond interaction with the standard compound MXM. Similarly, OWC, the reference compound for NIK, exhibited one H-bond of length 2.92 Å with E149 and three hydrophobic interactions (two with R84 and one with L198). However, compound C8 formed an H-bond interaction with D120 and eight different hydrophobic interactions. Whereas C4 formed one short H-bond of length 3.35 Å with L148, two long H-bond interactions with S152 (3.53 Å) and Q155 (3.52 Å), and five different hydrophobic interactions. Like OWC, algal-derived compounds formed common hydrophobic interactions with residues R84 and L198 of NIK. Overall, the comparison indicates that C4 and C8 show promising selectivity for the anti-inflammatory targets based on their binding interactions and formation of stabilizing H-bonds, hydrophobic, and salt bridges. C4 emerges as a strong drug-like candidate with optimal ADME properties and no Lipinski violations, while C8, despite its high lipophilicity, shows potent target engagement. These findings support the continued development of these algal-derived compounds as anti-inflammatory agents, with C4 offering a particularly favorable balance of drug-likeness and biological efficacy (Supplementary Table S2). Our docking results indicate that the algal-derived compounds C8 and C4 exploit similar physicochemical properties to effectively interact with key residues in the active sites of COX-1 and NIK. A similar kind of study has been performed by Rasouli et al. 2022,[47] where structure-based approaches were used to study the inhibitory activity of three protein kinases involved in Alzheimer's disease. This selectivity could be crucial for developing anti-inflammatory inhibitors, minimizing off-target effects in human cells.

3.2. MD simulation analysis

Molecular dynamics (MD) simulations provide insights into the dynamic behavior of protein-inhibitor interactions, revealing potential alterations in binding modes and the robustness of these interactions under physiological conditions. MD simulations also help in identifying any transient states that may enhance the inhibitory activity of compounds.[48,49] Hence, to evaluate the stability of the identified C4 and C8 compounds against both COX-1 and NIK, the docked complexes were simulated for 100 ns using the GROMACS 2022.2 package.

The Root Mean Square Deviation (RMSD) analysis provided insightful results, highlighting the selective binding of MXM, C8, and C4 compounds to COX-1 and OWC, C8 and C4 to the NIK, respectively (Fig. 2). In the initial 0–50 ns, all COX-1 complexes (MXM, C8, and C4) underwent a brief equilibration period. RMSD values gradually increased and stabilized, indicating the adaptation of ligands within the

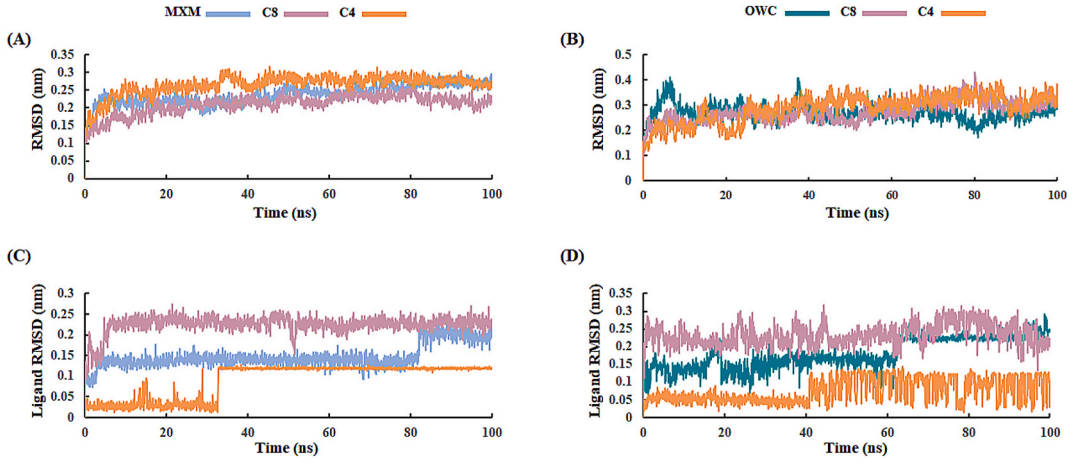


Fig. 2. Structural deviation of protein backbone and ligand throughout the simulation. (A) and (B) represent the RMSD profile of COX-1 and NIK, respectively. (C) and (D) represent the RMSD profile of each ligand when bound to COX-1 and NIK, respectively. Blue and green represent the reference compounds MXM and OWC for COX-1 and NIK. Purple and orange represent compounds C8 and C4, respectively. (For interpretation of the references to color in this figure legend, the reader is referred to the web version of this article.)

binding pocket. Among the protein-inhibitor complex systems, MXM, C8, and C4 exhibited an average protein backbone RMSD of 0.24, 0.21, and 0.26 nm, respectively, during the whole trajectory. Whereas the binding of OWC, C8, and C4 to the NIK receptor was characterized by a slight fluctuation during the initial 50 ns MD simulation but later stabilized with an average protein backbone RMSD of 0.27, 0.27 and 0.28 nm, respectively, indicating stable interactions. Overall, the binding of compounds C8 and C4 to both the receptors demonstrated no significant changes in the RMSD values of the protein backbone, as compared to their respective standard compounds, i.e., MXM and OWC for COX-1 and NIK, respectively. Notably, the binding of C8 and C4 to the NIK was characterized by more stable interactions than the standard OWC compound. This aligns with the molecular docking results, where these C8 and C4 compounds showed more favorable binding energies to the COX-1 and NIK, particularly C8 was unique in exhibiting low RMSD values with both COX-1 and NIK, suggesting that it binds more stably to the active site target. The RMSD profile of ligands bound to COX-1 and NIK complexes revealed that the C4 bound complexes show minor deviations throughout and appear more stable than the standard MXM and OWC complexes.

RMSF analysis was performed to assess the flexibility of individual amino acid residues within both COX-1 and NIK, as represented in Fig. 3. The RMSF values obtained ranged from 0.06 to 0.46 nm, reflecting moderate flexibility in various regions of both proteins. This analysis provides valuable insights into the mobility and flexibility of specific residues, enhancing our understanding of their functional roles within the protein structures upon ligand binding.[50] The binding of MXM, C8, and C4 with COX-1 exhibited a similar trend in most regions, whereas MXM caused higher RMSF values (0.28–0.46 nm) between the G96-I108 region and the E486-G496 region when it binds to COX1. In contrast, C8 binding led to reduced fluctuations (0.05–0.8 nm) in key active site residues Y355, S530, and R120, correlating with stronger binding affinity and suggesting enhanced conformational stabilization. C4 showed moderate rigidification, particularly at Y355. These regions correspond to functionally relevant domains, such as the membrane-binding and catalytic sites, thus warranting further structural mapping to determine their potential impact on enzymatic activity. A higher RMSF value indicates more flexible movements and fluctuations during the simulation.[51] In this regard, the C8 and C4 complexes with COX-1 do not contribute to any significant fluctuations in the system. Similarly, no significant fluctuations were observed in the NIK receptor when bound to OWC, C8, and C4 compounds. Remarkably, the loop region residues, the A41-T50 and the V82-G88 region of NIK, exhibited higher fluctuations (0.2–3.2 nm) when they bind to the algal-derived compounds (C8 and C4), compared to OWC, consistent with improved interaction at the ATP-binding cleft. These flexible regions are involved in regulatory or substrate recognition functions, suggesting that algal-derived compounds (C8 and C4) modulate protein function via induced local dynamics. These findings are significant, as they suggest compounds C8 and C4 from *C. vulgaris* could modulate COX-1 and NIK activity by acting as inhibitors, similar to known standard compounds MXM and OWC. These ligand-induced shifts, rigidification of COX-1′s Y355 & S530 and NIK's L148 & R84, enhance hydrogen bonding and π-π stacking, supporting persistent binding. Overall, RMSF data affirms that C8 and C4 promote structural stabilization of functionally important residues, underscoring their potential as dual-target anti-inflammatory agents. Further investigation into the structural and functional implications of these interactions is necessary to fully understand their therapeutic potential and develop new treatments for anti-inflammatory related diseases.

The radius of gyration gives us insights into the overall structure and compactness of the COX-1 and NIK complexes. Fig. 4A and B represent the Rg values of the protein backbone of both receptors when they bind to the selected compounds. From the results obtained, the calculated average radius of gyration values for COX-1-MXM, COX-1-C8, and COX-1-C4 complexes are found to be 2.42 nm, 2.44 nm, and 2.43 nm, respectively. In the case of NIK-OWC, NIK-C8, and NIK-C4 complexes, the average radius of gyration values is found to be 2.12 nm, 2.14 nm, and 2.16 nm, respectively. Fig. 4A shows a consistent trend in the radius of gyration for COX-1-C4 and NIK-C4 complexes through time, indicating greater compactness. In contrast, the COX-1-MXM and COX-1-C8 complexes remained compact throughout the simulation. The estimated average radius of gyration values for C8 and C4 compounds with the COX-1 and NIK complexes show that ligand interaction leads to protein stabilization and enhanced compactness. This implies that the presence of ligands aids in the structural stability of protein complexes.

The overall capacity of the protein to interact with other molecules and the degree of expansion in protein volume is determined by Solvent accessible surface area.[52] Fig. 4C and D demonstrate the Solvent accessible surface area analysis of the complexes. The analysis revealed that the average SASA values from the whole trajectory for COX-1-MXM, COX-1-C8, and COX-1-C4 complexes are 250.91 nm^2, 255.80 nm^2, and 253.90 nm^2, respectively. Similarly, NIK-MXM, NIK-C8, and NIK-C4 complexes exhibited average SASA values of 178.11 nm^2, 180.57 nm^2, and 180.34 nm^2, respectively. The results showed that the complexes formed by C8 and C4 with COX-1 and NIK show more SASA trends after the binding of inhibitors. The SASA analysis revealed substantial differences, indicating a considerable loss of hydrophobic contact within the residues of the C8 and C4 with COX-1 and NIK complexes. This suggests that the C8 and C4 compounds had a major impact on the hydrophobic interactions within the COX-1 and NIK complexes. The exploration of conformational geometry by examining the SASA of C8 and C4 ligand-bound complexes demonstrated that these inhibitors may affect the overall conformation of COX-1 and NIK.

The conformational stability of the complexes can be examined by the number of intramolecular hydrogen bonds (the donor–acceptor distance was $\leq$ 3.5 Å or, 0.35 nm and the hydrogen–donor acceptor angle was $\geq$ 120°) formed between the inhibitors and both receptors COX-1 and NIK over the 100 ns trajectory, and hydrogen bonds at specific positions are necessary conditions for binding (Fig. 5). MXM and C8 ligand-bound complexes maintained 1 to 2 stable hydrogen bonds throughout the entire MD trajectories, whereas the C4 ligand-bound

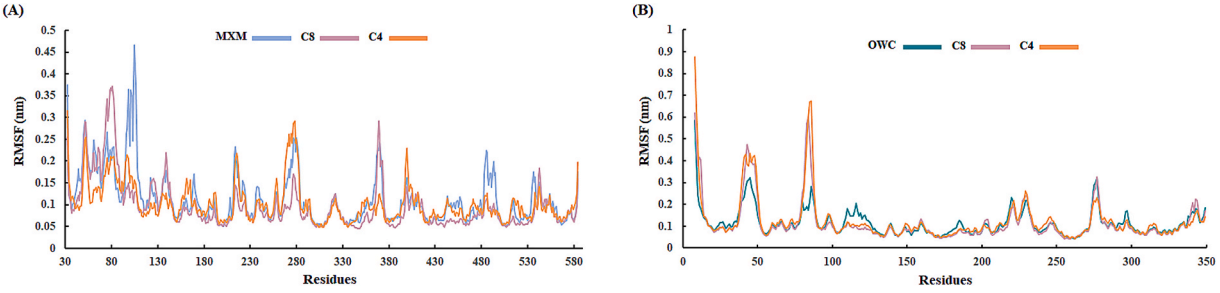


Fig. 3. Residual fluctuations throughout the simulation. (A) and (B) represent the RMSF profile of each amino acid upon ligand binding to COX-1 and NIK, respectively. Blue and green represent the reference compounds MXM and OWC for COX-1 and NIK. Purple and orange represent compounds C8 and C4, respectively. (For interpretation of the references to color in this figure legend, the reader is referred to the web version of this article.)

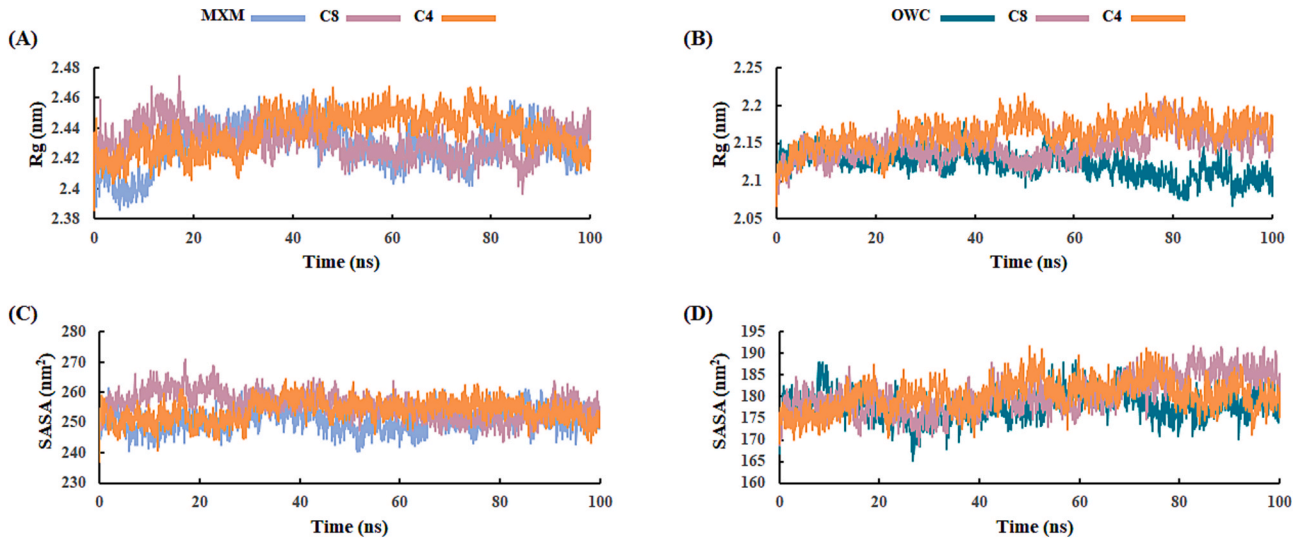


Fig. 4. Rg and SASA profile each receptor upon ligand binding. Blue and green represent the reference compounds MXM and OWC for COX-1 and NIK. Purple and orange represent compounds C8 and C4, respectively. (For interpretation of the references to color in this figure legend, the reader is referred to the web version of this article.)

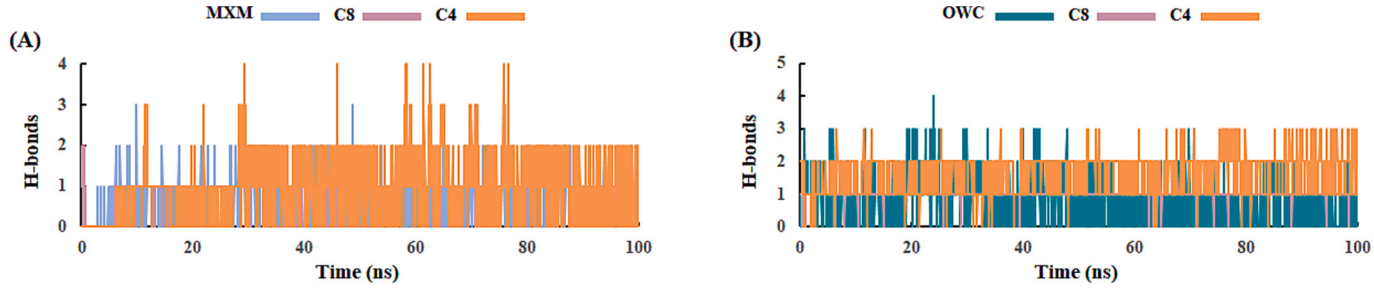


Fig. 5. Changes in the number of hydrogen bonds between protein–ligand complexes throughout the simulation. Blue and green represent the reference compounds MXM and OWC for COX-1 and NIK. Purple and orange represent compounds C8 and C4, respectively. (For interpretation of the references to color in this figure legend, the reader is referred to the web version of this article.)

complex had several potential hydrogen bonds up to 3 with the COX-1 receptor. This stability correlates well with their strong interaction energy profiles and low RMSD values for COX-1. Simultaneously, the average number of intramolecular hydrogen bonds in the NIK-OWC, NIK-C8, and NIK-C4 complexes 1, 1, and 2, respectively. This aligns with its relatively more hydrogen bonds than the standard compounds and stable RMSD values for the COX-1 and NIK, suggesting that while it may not form as many immediate interactions, but the binding of C8 and C4 remains stable over time.

3.3. Secondary structure analysis

To correlate residue flexibility with conformational dynamics, DSSP-based secondary structure analysis was conducted following the approach of Rasouli et al. 2017,[53] providing structural context during MD simulations. In the COX-1 systems, consistent α-helical regions (residues 100–200, 300–450) were observed across all complexes (MXM, C8, and C4) depicted in Supplementary Fig. S1. The C8-COX-1 complex exhibited greater structural integrity, marked by limited transitions and increased β-sheet content (residues 250–300), indicative of stabilizing ligand interactions. In contrast, the C4 complex displayed moderate flexibility, particularly in loop regions (residues 200–250), which alternated between coil and turn conformations, correlating with its intermediate binding energy (–4.359 kcal/mol) compared to C8 (–8.625 kcal/mol). For NIK complexes depicted in Supplementary Fig. S2, the OWC reference displayed notable secondary structure disruptions, especially in residues 150–250, with frequent α-helix to coil transitions, reflecting its weaker binding (–2.628 kcal/mol). The C8-NIK complex retained robust α-helical structure and reduced fluctuations in dynamic regions, supporting its superior affinity (–6.798 kcal/mol). C4-NIK displayed localized terminal flexibility while preserving core structure. These findings highlight that C8 and C4 enhance protein stability in both COX-1 and NIK, explaining their improved binding profiles. DSSP analysis thus substantiates the structural basis for ligand efficacy and supports the potential of these algal-derived inhibitors in targeted drug design.

3.4. Essential dynamics

To understand the concentrated global motions during the simulation, principal components analysis (PCA) analysis was performed where the first 25 eigenvectors were used to determine the eigenvalues and percentage change in the movement protein backbone of each eigenvector from the last 50 ns trajectory of the simulation. The first 5 principal components (PCs) for COX-1 bound to MXM, C8, and C4 and NIK bound to OWC, C8, and C4 exhibited the most extensive motions compared to other PCs and represented Fig. 6A and B. The first 2 PCs showed a cumulative variance of 30.69, 26.41, and 41.46 % COX-1 when they bind to MXM, C8, and C4, respectively. In the other case, the first 2 PCs exhibited a cumulative variance of 35.64, 38.75, and 38.54 % for NIK when they bind to OWC, C8, and C4, respectively. Moreover, the projections of the first 2 PCs were generated

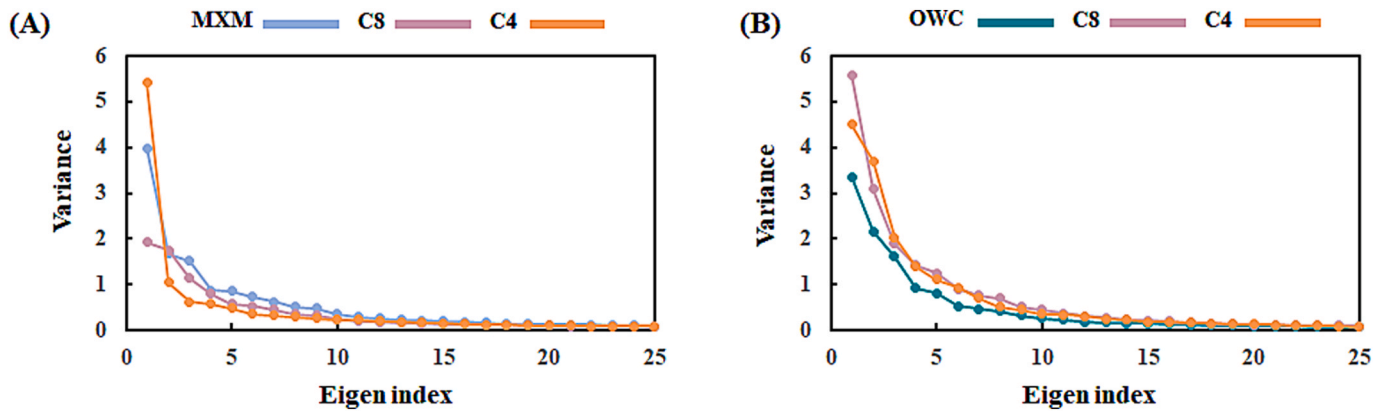


Fig. 6. Principal component analysis of protein backbone of both receptors upon ligand binding from the last 50 ns trajectory information. Blue and green represent the reference compounds MXM and OWC for COX-1 and NIK. Purple and orange represent compounds C8 and C4, respectively. (For interpretation of the references to color in this figure legend, the reader is referred to the web version of this article.)

(Supplementary Fig. S3) for both the receptors.

To understand the conformational space and protein dynamics in terms of the Free energy landscape, the top 2 eigenvectors with cosine values less than 0.2 were utilized. The C8 and C4 complex structures show lesser eigenvalues when compared to the standard MXM and OWC bound complexes, which signifies a reduction in the overall motion of the proteins during the simulation period (Figs. 7A and 8A). The energy scale and the extent of FEL sampled by COX-1-MXM, COX-1-C8, and COX-1-C4 differ. The structure of COX-1-MXM evolves over a larger extent of FEL with three minimum energy basins, whereas the COX-1-C8 and COX-1-C4 samples over a significantly spread FEL with one and two minimum energy basins, respectively. Similarly, all three NIK complexes have one minimum energy basin, but NIK-C4 is involved in lower amplitude motions.

For further analysis, the stable conformations of (i) COX-1-MXM, COX-1-C8, and COX-1-C4 were extracted at 96 ns, 83 ns, and 99 ns, respectively, and (ii) the same for NIK-OWC, NIK-C8, and NIK-C4 are extracted at 82 ns, 72 ns, and 83 ns, respectively. Figs. 7B and 8B depict the superimposition of (i) COX-1-MXM, COX-1-C8, and COX-1-C4 with the initial configuration having an RMSD of 1.919, 1.117, and 1.943 nm and (ii) NIK-OWC, NIK-C8 and NIK-C4 from clusters with the initial configuration having a RMSD of 1.254, 1.506 and 1.744 nm, respectively. The conformations belong to different dynamics states, in which the purple region reveals minimal dynamics while other regions are involved in higher amplitude motions. C8 and C4 bound complexes are corroborated with the confined dynamics attributed to the reduced residue fluctuations. The Ramachandran plots of both COX-1 and NIK proteins maintain stable conformations when bound to their respective compounds during the last 50 ns of the trajectory. The predominant clustering of data points within the favored regions (alpha-helical and beta-sheet) signifies well-preserved secondary structures, indicating stable protein–ligand interactions (Supplementary Fig. S4).

3.5. *Binding free energy analysis*

The molecular mechanics Poisson Boltzmann surface area is one of the most commonly used methods for investigating the binding behavior of biomolecular complexes.[45,46,54] The complexes formed by COX-1-

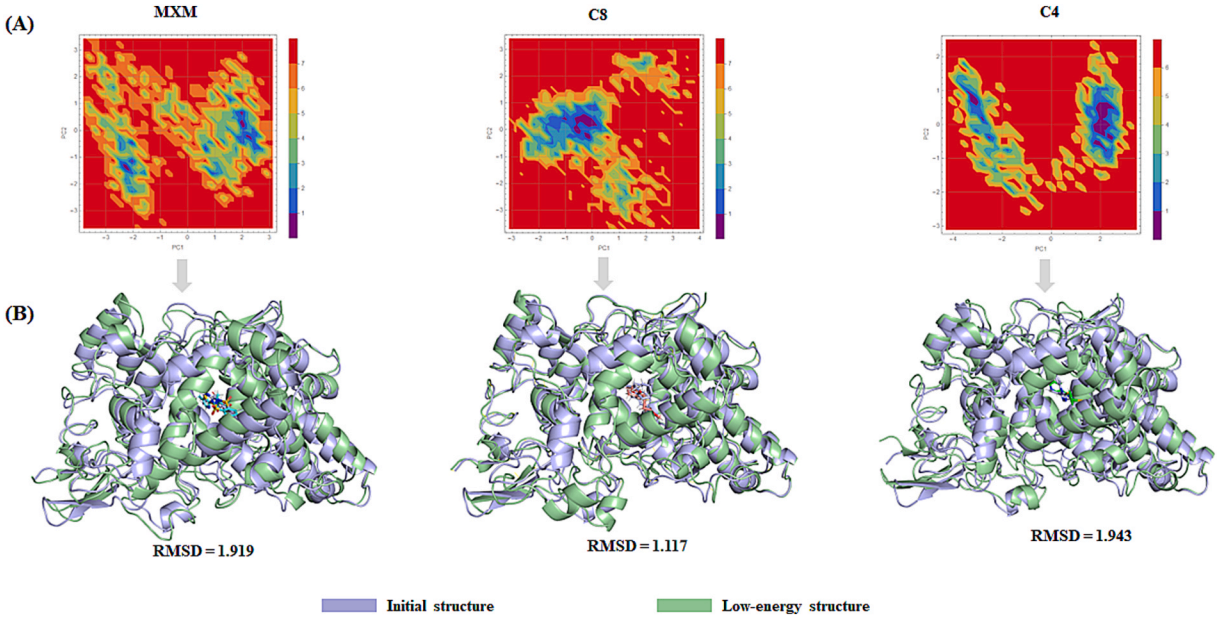


Fig. 7. Gibbs' free energy landscapes of COX-1 when bound to MXM, C8, and C4. (A) Low energy systems were indicated in deep blue color. (B) Superimposition of initial configuration and low-energy structures of COX-1. (For interpretation of the references to color in this figure legend, the reader is referred to the web version of this article.)

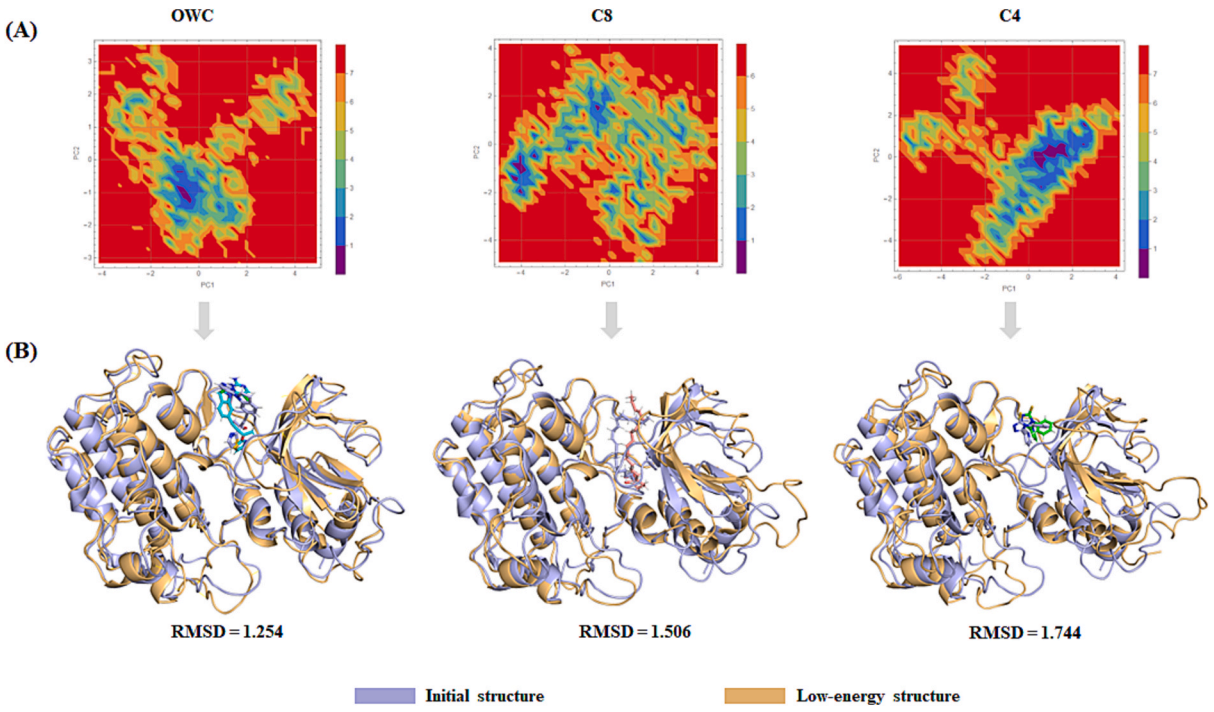


Fig. 8. Gibbs' free energy landscapes of NIK when bound to OWC, C8, and C4. (A) Low energy systems were indicated in deep blue color. (B) Superimposition of initial configuration and low-energy structures of NIK. (For interpretation of the references to color in this figure legend, the reader is referred to the web version of this article.)

MXM, COX-1-C8, and COX-1-C4, along with NIK-OWC, NIK-C8, and NIK-C4, were further explored using the MM-PBSA free energy calculations. The average ΔG_{bind} of all the complexes is displayed in Supplementary Table S3, and it can be observed that the lead compounds C8 bound complexes have a high negative binding affinity towards COX-1 as well as NIK (Fig. 9). The top compound C8 displays higher negative binding free energy, i.e., −172.489 KJ/mol and −100.865 KJ/mol with COX-1 and NIK, respectively, when compared to the standard compounds MXM and OWC, i.e., −108.598 KJ/mol and −81.303 KJ/mol. C4 also proves to be a better inhibitor that exhibits similar binding, i.e., −79.868 KJ/mol and −71.41 KJ/mol with the COX-1 and NIK receptors.

The per-residue energy contributions for the complexes formed by COX-1-MXM, COX-1-C8, and COX-1-C4, along with NIK-OWC, NIK-C8, and NIK-C4, are displayed in Supplementary Fig. S5. During the interaction of C8 and C4 with COX-1, the residues which are mainly contributing to the negative energy are V116, L117, F205, V344, Y348, V349, L352, P381, Y385, W387, P518, I523, G526, A527, L531, and L534. Notably, these residues are well-established for their roles in NSAID binding through hydrogen bonding or water-mediated interactions appear crucial in ligand stabilization, as also supported by crystallographic studies of meloxicam and isoxicam binding. In the case of the interaction between C8 and C4 with NIK, the residues that contribute to negative binding free energy are V82, D89, V90, A103, M145, L147, G150, G151, L198, R205, and C209. These amino acids are situated within or proximal to the ATP-binding and regulatory domains of NIK, indicating their direct involvement in modulating ligand affinity and potential kinase inhibition. The results suggest that the stability of all the complexes formed by the Standard (MXM and OWC) and top compounds (C8 and C4) with COX-1 and NIK proteins is mainly due to van der Waals and electrostatic interactions. The MM-PBSA results underscore the biological significance of these conserved residues within the active sites, confirming their roles in stabilizing ligand-receptor interactions critical for anti-inflammatory and in the binding between the lead phytochemicals and the anti-inflammatory receptors. While MM-PBSA provides valuable insight into ligand binding, it is important to note that entropy contributions particularly conformational and solvation entropy were not included in the free energy estimations. This omission is a recognized limitation of the method. Nevertheless, the relative ranking of compounds remains reliable for comparative purposes. These findings provide a structural rationale for the observed

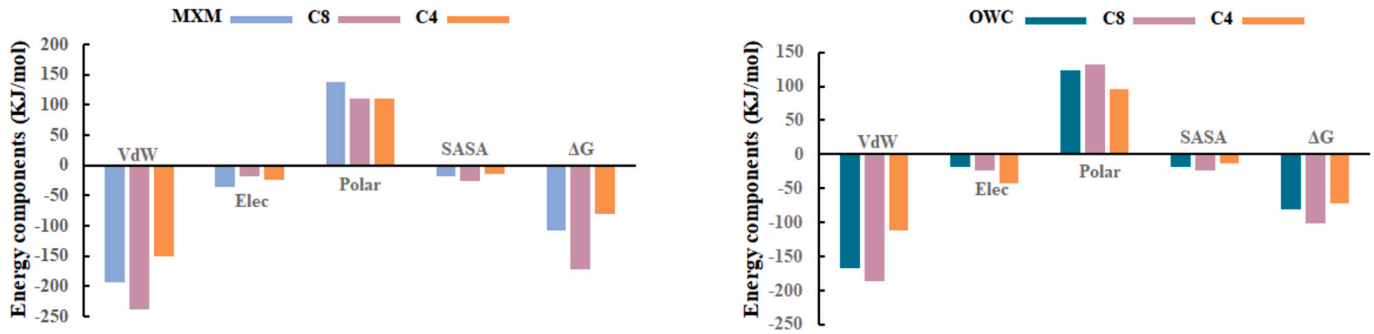


Fig. 9. Free energy components in KJ/mol. Blue and green represent the reference compounds MXM and OWC for COX-1 and NIK. Purple and orange represent compounds C8 and C4, respectively.

inhibitory effects and inform the rational design of next-generation therapeutic agents targeting COX-1 and NIK.

4. Conclusions

The prevalence of adverse effects associated with synthetic anti-inflammatory drugs underscores the need for alternative therapeutic strategies. Natural products, especially those derived from marine organisms like *C. vulgaris*, offer a promising avenue. Therefore, this study aimed to evaluate the anti-inflammatory activity of potential lead compounds from the methanolic extract of *C. vulgaris* by targeting COX-1 and NIK, two key receptors implicated in the inflammatory process. Molecular docking analysis identified several C. vulgaris compounds with strong binding affinities for both targets. Among these, compounds C8 and C4, possessing desirable drug-like properties, exhibited significant potential as selective inhibitors. Molecular dynamics simulations further supported these findings, showing stable interactions between the compounds and the target proteins. The analysis of RMSD, RMSF, Rg, and SASA provided insights into the conformational stability and dynamic behavior of the protein–ligand complexes. The free energy calculations using MM-PBSA revealed that the C8 and C4 compounds exhibited favorable binding energies, suggesting their potential as potent inhibitors. The analysis of per-residue energy contributions identified key amino acid residues that contribute to the stability of the protein–ligand complexes. To substantiate these computational findings, subsequent investigations employing experimental validation are imperative. To fully elucidate the therapeutic potential and safety profile of the identified compounds, particularly C8 and C4, further experimental validation, including in vitro and in vivo studies followed by clinical trials, is necessary. This dual targeting approach, inhibiting both COX-1 and NIK, presents a promising strategy for developing novel anti-inflammatory therapies with reduced side effects.

5. Fundings

This work was supported by the National Research Foundation of Korea (NRF) grant funded by the Korea government (MSIT) (No. NRF-2022R1A2C4002510).

CRediT authorship contribution statement

Mahesh Samantaray: Writing – original draft, Investigation, Formal analysis. **Sthitaprajna Sahoo:** Writing – original draft, Investigation, Formal analysis, Conceptualization. **Durga Prasad Sahoo:** Writing – review & editing, Formal analysis. **Guneswar Sethi:** Writing – review & editing, Formal analysis. **Sarman Singh:** Writing – review & editing, Supervision, Formal analysis. **Hak-Kyo Lee:** Writing – review & editing, Supervision. **Biswajita Pradhan:** Writing – review & editing, Supervision, Conceptualization. **Donghyun Shin:** Writing – review & editing, Supervision, Conceptualization.

Declaration of competing interest

The authors declare that they have no known competing financial interests or personal relationships that could have appeared to influence the work reported in this paper.

Acknowledgments

The authors thank Jeonbuk National University, Pondicherry University, and Aarupadai Veedu Medical College & Hospital for providing all the resources needed to pursue this research.

6. *Data availability statement*

The raw MD trajectory data of this study are publicly available on Zenodo (https://zenodo.org/) with accession number (Doi: 10.5281/zenodo.15654244).

Appendix A. Supplementary data

Supplementary data to this article can be found online at https://doi.org/10.1016/j.jgeb.2025.100531.

References

1. Dhingra AK, Chopra B. Inflammation as a therapeutic target for various deadly disorders: a review. *Curr Drug Targets.* 2020;21:582–588. https://doi.org/10.2174/1389450120666191204154115.
2. Buckley CD. Why does chronic inflammatory joint disease persist? *Clin Med (Lond).* 2003;3:361–366. https://doi.org/10.7861/clinmedicine.3-4-361.
3. Lawrence T, Gilroy DW. Chronic inflammation: a failure of resolution? *Int J Exp Pathol.* 2007;88:85–94. https://doi.org/10.1111/j.1365-2613.2006.00507.x.
4. Natarajan R, Nadler JL. Lipid inflammatory mediators in diabetic vascular disease. *Arterioscler Thromb Vasc Biol.* 2004;24:1542–1548. https://doi.org/10.1161/01.ATV.0000133606.69732.4c.
5. El Sayed MT, El-Sharief MAMS, Zarie ES, et al. Design, synthesis, anti-inflammatory antitumor activities, molecular modeling and molecular dynamics simulations of potential naprosyn® analogs as COX-1 and/or COX-2 inhibitors. *Bioorg Chem.* 2018;76:188–201. https://doi.org/10.1016/j.bioorg.2017.11.002.
6. Beura S, Chetti P. Identification of potential human COX-2 inhibitors using computational modeling and molecular dynamics simulations. *J Mol Struct.* 2020;1216, 128271. https://doi.org/10.1016/j.molstruc.2020.128271.
7. Anti-inflammatory potential of selective small compounds by targeting TNF-α & NF-kB signaling: a comprehensive molecular docking and simulation study. J Biomol Struct Dyn. 41(23), n.d. https://www.tandfonline.com/doi/abs/10.1080/07391102.2023.2196692 (accessed November 21, 2024).
8. Cheemanapalli S, Chinthakunta N, Shaikh NM, Shivaranjani V, Pamuru RR, Chitta SK. Comparative binding studies of curcumin and tangeretin on up-stream elements of NF-kB cascade: a combined molecular docking approach. *Netw Model Anal Health Inform Bioinforma.* 2019;8:15. https://doi.org/10.1007/s13721-019-0196-2.
9. Na YR, Yoon YN, Son D, Jung D, Gu GJ, Seok SH. Consistent inhibition of cyclooxygenase drives macrophages towards the inflammatory phenotype. *PLoS One.* 2015;10, e0118203. https://doi.org/10.1371/journal.pone.0118203.
10. Frölich JC, Stichtenoth DO. Renal side effects of NSAIDs: role of COX-1 and COX-2. In: Vane J, Botting J, editors. Selective COX-2 Inhibitors: Pharmacology, Clinical Effects and Therapeutic Potential, Dordrecht: Springer Netherlands; 1998, p. 87–98. Doi: 10.1007/978-94-011-4872-6_9.
11. Seibert K, Zhang Y, Leahy K, Hauser S, Masferrer J, Isakson P. Distribution of Cox-1 and Cox-2 in Normal and Inflamed Tissues. In: Honn KV, Nigam S, Marnett LJ, editors. Eicosanoids and Other Bioactive Lipids in Cancer, Inflammation, and Radiation Injury 2: Part A, Boston, MA: Springer US; 1997, p. 167–70. Doi: 10.1007/978-1-4615-5325-0_24.
12. Willoughby DA, Moore AR, Colville-Nash PR. COX-1, COX-2, and COX-3 and the future treatment of chronic inflammatory disease. *Lancet.* 2000;355:646–648. https://doi.org/10.1016/S0140-6736(99)12031-2.
13. UCVM Class of 2016, Banse H, Cribb AE. Comparative efficacy of oral meloxicam and phenylbutazone in 2 experimental pain models in the horse. Can Vet J. 2017;58:157–67.
14. Said MF, Moussa BA, Mahrouse MA, Marie SM, Mohamed NM. Exploring new imines as anti-inflammatory COX and 5-LOX inhibitors with an improved pharmacokinetic profile. *Future Med Chem.* 2024;16:311–334. https://doi.org/10.4155/fmc-2023-0280.
15. Noble SL, King DS, Olutade JI. Cyclooxygenase-2 enzyme inhibitors: place in therapy. *Am Fam Physician.* 2000;61:3669–3676.
16. Pflug KM, Sitcheran R. Targeting NF-κB-inducing kinase (NIK) in immunity, inflammation, and cancer. *Int J Mol Sci.* 2020;21, 8470. https://doi.org/10.3390/ijms21228470.
17. Kucharzewska P, Maracle CX, Jeucken KCM, et al. NIK–IKK complex interaction controls NF-κB-dependent inflammatory activation of endothelium in response to LTβR ligation. *J Cell Sci.* 2019;132, jcs225615. https://doi.org/10.1242/jcs.225615.
18. Tak PP, Firestein GS. NF-κB: a key role in inflammatory diseases. *J Clin Invest.* 2001;107:7–11.
19. Rainsford KD. Profile and mechanisms of gastrointestinal and other side effects of nonsteroidal anti-inflammatory drugs (NSAIDs). *Am J Med.* 1999;107:27–35. https://doi.org/10.1016/S0002-9343(99)00365-4.
20. Valero-Vello M, Peris-Martínez C, García-Medina JJ, et al. Searching for the antioxidant, anti-inflammatory, and neuroprotective potential of natural food and nutritional supplements for ocular health in the Mediterranean population. *Foods.* 2021;10:1231. https://doi.org/10.3390/foods10061231.
21. Pradhan B, Patra S, Behera C, et al. Preliminary investigation of the antioxidant, anti-diabetic, and anti-inflammatory activity of enteromorpha intestinalis extracts. *Molecules.* 2021;26:1171. https://doi.org/10.3390/molecules26041171.
22. Pradhan B, Bhuyan PP, Ki J-S. Immunomodulatory, antioxidant, anticancer, and pharmacokinetic activity of Ulvan, a seaweed-derived sulfated polysaccharide: an updated comprehensive review. *Mar Drugs.* 2023;21:300. https://doi.org/10.3390/md21050300.

23. Pradhan B, Ki J-S. Phytoplankton toxins and their potential therapeutic applications: a journey toward the quest for potent pharmaceuticals. *Mar Drugs.* 2022;20:271. https://doi.org/10.3390/md20040271.
24. Pradhan B, Ki J-S. Biological activity of algal derived carrageenan: a comprehensive review in light of human health and disease. *Int J Biol Macromol.* 2023;238, 124085. https://doi.org/10.1016/j.ijbiomac.2023.124085.
25. Pradhan B, Ki J-S. Antioxidant and chemotherapeutic efficacies of seaweed-derived phlorotannins in cancer treatment: a review regarding novel anticancer drugs. *Phytother Res.* 2023;37:2067–2091. https://doi.org/10.1002/ptr.7809.
26. Pradhan B, Rout L, Ki J-S. Immunomodulatory and anti-inflammatory and anticancer activities of porphyran, a sulfated galactan. *Carbohydr Polym.* 2023;301, 120326. https://doi.org/10.1016/j.carbpol.2022.120326.
27. Pradhan B, Nayak R, Patra S, Jit BP, Ragusa A, Jena M. Bioactive metabolites from marine algae as potent pharmacophores against oxidative stress-associated human diseases: a comprehensive review. *Molecules.* 2021;26:37. https://doi.org/10.3390/molecules26010037.
28. Sahoo S, Samantaray M, Jena M, et al. In vitro and in silico studies to explore potent antidiabetic inhibitor against human pancreatic alpha-amylase from the methanolic extract of the green microalga Chlorella vulgaris. *J Biomol Struct Dyn.* 2024;42:8089–8099. https://doi.org/10.1080/07391102.2023.2244592.
29. Elbouzidi A, Taibi M, Laaraj S, et al. Chemical profiling of volatile compounds of the essential oil of grey-leaved rockrose (Cistus albidus L.) and its antioxidant, anti-inflammatory, antibacterial, antifungal, and anticancer activity in vitro and in silico. *Front Chem.* 2024;12. https://doi.org/10.3389/fchem.2024.1334028.
30. Xu S, Hermanson DJ, Banerjee S, et al. Oxicams bind in a novel mode to the cyclooxygenase active site via a two-water-mediated H-bonding network*. *J Biol Chem.* 2014;289:6799–6808. https://doi.org/10.1074/jbc.M113.517987.
31. de Leon-Boenig G, Bowman KK, Feng JA, et al. The crystal structure of the catalytic domain of the NF-κB inducing kinase reveals a narrow but flexible active site. *Structure.* 2012;20:1704–1714. https://doi.org/10.1016/j.str.2012.07.013.
32. Waterhouse A, Bertoni M, Bienert S, et al. SWISS-MODEL: homology modelling of protein structures and complexes. *Nucleic Acids Res.* 2018;46:W296–W303. https://doi.org/10.1093/nar/gky427.
33. Daina A, Michielin O, Zoete V. SwissADME: a free web tool to evaluate pharmacokinetics, drug-likeness and medicinal chemistry friendliness of small molecules. *Sci Rep.* 2017;7, 42717. https://doi.org/10.1038/srep42717.
34. Bekker H, Berendsen H, Dijkstra E, Achterop S, Vondrumen R, Vanderspoel D, et al. Gromacs - a parallel computer for molecular-dynamics simulations. In: 4th International Conference on Computational Physics (PC 92). PHYSICS COMPUTING '92 1993:252–6.
35. Van Der Spoel D, Lindahl E, Hess B, Groenhof G, Mark AE, Berendsen HJC. GROMACS: fast, flexible, and free. *J Comput Chem.* 2005;26:1701–1718. https://doi.org/10.1002/jcc.20291.
36. Huang J, MacKerell AD. CHARMM36 all-atom additive protein force field: validation based on comparison to NMR data. *J Comput Chem.* 2013;34:2135–2145. https://doi.org/10.1002/jcc.23354.
37. Vanommeslaeghe K, MacKerell Jr AD. Automation of the CHARMM general force field (CGenFF) I: bond perception and atom typing. *J Chem Inf Model.* 2012;52:3144–3154. https://doi.org/10.1021/ci300363c.
38. Meza JC. Steepest descent. *WIREs Comput Stat.* 2010;2:719–722. https://doi.org/10.1002/wics.117.
39. Bussi G, Donadio D, Parrinello M. Canonical sampling through velocity rescaling. *J Chem Phys.* 2007;126, 014101. https://doi.org/10.1063/1.2408420.
40. Parrinello M, Rahman A. Polymorphic transitions in single crystals: a new molecular dynamics method. *J Appl Phys.* 1981;52:7182–7190. https://doi.org/10.1063/1.328693.
41. Sahoo S, Lee H-K, Shin D. Structure-based virtual screening and molecular dynamics studies to explore potential natural inhibitors against 3C protease of foot-and-mouth disease virus. *Front Vet Sci.* 2024;10.
42. Sahoo S, Purohit P, Samantaray S, Meher BR. Identification of antiviral phytocompounds as potential anti-dengue agents against DENV NS2B/NS3 protease: an integrated molecular modelling and dynamics approach. *ChemistrySelect.* 2024;9, e202400384. https://doi.org/10.1002/slct.202400384.
43. Sahoo S, Gosu V, Lee H-K, Shin D. Deciphering the conformational changes induced by high-risk nsSNPs in β-lactoglobulin. *Heliyon.* 2024;10. https://doi.org/10.1016/j.heliyon.2024.e40040.
44. Sahoo S, Lee H-K, Shin D. Elucidating the structural dynamics induced by active site mutations in 3C protease of foot-and-mouth disease virus. *PLoS One.* 2025;20, e0321079. https://doi.org/10.1371/journal.pone.0321079.
45. Genheden S, Ryde U. The MM/PBSA and MM/GBSA methods to estimate ligand-binding affinities. *Expert Opin Drug Discov.* 2015;10:449–461. https://doi.org/10.1517/17460441.2015.1032936.
46. Kumari R, Kumar R, Lynn A. g_mmpbsa—a GROMACS tool for high-throughput MM-PBSA calculations. *J Chem Inf Model.* 2014;54:1951–1962. https://doi.org/10.1021/ci500020m.
47. Rasouli H, Ghazvini H, Bagher SM, Yarani R, Altıntaş AJ, Nikoo SG, Ramalho TC. Deciphering inhibitory activity of flavonoids against tau protein kinases: a coupled molecular docking and quantum chemical study. *J Biomol Struct Dyn.* 2022;40:411–424. https://doi.org/10.1080/07391102.2020.1814868.
48. Zhao Z, Zhao L, Kong C, Zhou J, Zhou F. A review of biophysical strategies to investigate protein-ligand binding: what have we employed? *Int J Biol Macromol.* 2024;276, 133973. https://doi.org/10.1016/j.ijbiomac.2024.133973.
49. Zia SR, Coricello A, Bottegoni G. Increased throughput in methods for simulating protein ligand binding and unbinding. *Curr Opin Struct Biol.* 2024;87, 102871. https://doi.org/10.1016/j.sbi.2024.102871.
50. Arumugam S, Muthuvel R, Anjugam C, Kulanthaivel L, Subbaraj GK. Challenges and opportunities for analyzing protein–ligand interactions. In: Patel A, ed. *Biochemical Techniques for Analyzing Protein-Lipid Interactions*. Singapore: Springer Nature; 2024:1–20. https://doi.org/10.1007/978-981-97-5437-3_1.
51. Shukla R, Tripathi T. Molecular dynamics simulation of protein and protein–ligand complexes. In: Singh DB, ed. *Computer-Aided Drug Design*. Singapore: Springer; 2020:133–161. https://doi.org/10.1007/978-981-15-6815-2_7.
52. Du X, Li Y, Xia Y-L, et al. Insights into protein–ligand interactions: mechanisms, models, and methods. *Int J Mol Sci.* 2016;17:144. https://doi.org/10.3390/ijms17020144.
53. Rasouli H, Mehrabi M, Arab SS, Khodarahmi R. Are Pro8/Pro18 really critical for functional dynamic behavior of human endostatin N-terminal peptide? A comparative molecular dynamics study. *J Iran Chem Soc.* 2017;14:2023–2039. https://doi.org/10.1007/s13738-017-1140-y.
54. Poli G, Granchi C, Rizzolio F, Tuccinardi T. Application of MM-PBSA methods in virtual screening. *Molecules.* 2020;25:1971. https://doi.org/10.3390/molecules25081971.